ELSEVIER

Journal of Structural Geology 25 (2003) 1993–2003

JOURNAL OF STRUCTURAL GEOLOGY

www.elsevier.com/locate/jsg

Simple shear of deformable square objects

Susan H. Treagus[a,*], Labao Lan[b]

[a]*Department of Earth Sciences, University of Manchester, Manchester M13 9PL, UK*
[b]*IRI/Lamont-Doherty Earth Observatory, Columbia University, Palisades, NY 10964-8000, USA*

Received 9 October 2002; received in revised form 21 February 2003; accepted 24 February 2003

Abstract

Finite element models of square objects in a contrasting matrix in simple shear show that the objects deform to a variety of shapes. For a range of viscosity contrasts, we catalogue the changing shapes and orientations of objects in progressive simple shear. At moderate simple shear ($\gamma = 1.5$), the shapes are virtually indistinguishable from those in equivalent pure shear models with the same bulk strain ($R_S = 4$), examined in a previous study. In theory, differences would be expected, especially for very stiff objects or at very large strain. In all our simple shear models, relatively competent square objects become asymmetric barrel shapes with concave shortened edges, similar to some types of boudin. Incompetent objects develop shapes surprisingly similar to mica fish described in mylonites.

Keywords: Simple shear; Numerical modelling; Objects in a matrix

1. Introduction

One of the fundamental questions for structural geologists to answer is whether the geometry of rock structures can reveal the kinematics of the deformation. For example, are the fabrics and structures that arise from simple shear of rocks *necessarily* very different from those that arise in pure shear? If the structures in question arise only from strain, in theory there should be no difference, because the distortion associated with simple shear can be considered as pure shear plus rotation (see Hobbs et al., 1976, fig. 1.14). However, in a mechanically active system, the vorticity of the deformation is likely to affect the development of deformation structures. For example, it is well known that rigid objects in a linearly viscous matrix rotate differently in pure shear than in simple shear (Ghosh and Ramberg, 1976).

This paper concerns the two-dimensional behaviour of *ductile square objects* in a contrasting matrix, in simple shear, forming a sequel to a recent study of square objects in pure shear (Treagus and Lan, 2000). Most studies of geological objects or inclusions have concerned elliptical shapes, with studies of simple shear concentrating on rigid objects in a viscous matrix. However, a number of geological objects may be approximated to square-shaped for the purpose of modelling their deformation: for example, angular grains or clasts, prismatic porphyroclasts, and initially rectilinear boudins. An important point of principle is that non-elliptical objects deform to irregular shapes that reflect rheological contrasts, whereas elliptical objects will deform to other elliptical shapes (Treagus et al., 1996).

Several recent studies of rigid objects in a matrix in simple shear have sought to explain the orientation of porphyroclasts in natural shear zones (Arbaret et al., 2001; Mancktelow et al., 2002; ten Grotenhuis et al., 2002; Marques and Coelho, 2003). However, in this paper, we are concerned with *deformable objects* in a matrix. It is well-known that a linearly viscous elliptical object coherently embedded in a contrasting linearly viscous matrix undergoes a different strain from the bulk strain, which is inversely proportional to the object/matrix viscosity ratio (Eshelby, 1957; Gay, 1968a; Bilby et al., 1975; Shimamoto, 1975). However, applications of these theories to the deformation of rocks (e.g. Gay, 1968b; Lisle et al., 1983; Freeman, 1987; Treagus and Treagus, 2002) rely mainly on the algebraic relationship of object to matrix strain relationships derived for pure shear by Gay (1968a) or Bilby et al. (1975). Bilby and Kolbuszewski (1977) have demonstrated different behavioural effects for elliptical

* Corresponding author. Tel.: +44-161-275-3822; fax: +44-161-275-3947.
E-mail address: s.treagus@man.ac.uk (S.H. Treagus).

0191-8141/03/$ - see front matter © 2003 Elsevier Ltd. All rights reserved.
doi:10.1016/S0191-8141(03)00049-X

inclusions in simple shear, although their results for finite strain are not easily comparable with those for pure shear.

In simple shear, whether elliptical objects strain continuously, or rotate and oscillate within deformation bounds, or undergo no strain or rotation (steady behaviour), depends partly on initial ellipticity, but mainly on the balance between the viscosity ratio and the vorticity of the deformation (Bilby and Kolbuszewski, 1977). These authors define three regimes of behaviour in simple shear: in *regime 1* (viscosity ratio, $m < 2$), all objects deform progressively towards greater ellipticity; in *regime 2* ($2 < m < \sim 3.4$), some objects progressively deform and others oscillate; in *regime 3*($m > 3.4$), all objects undergo deformation within limits, in cycles of oscillating rotation, deformation and shape change. These cycles have γ wavelength values of ~ 10, over which deformation the elliptical objects deform and then undeform, while rotating. Weijermars (1993) used the term 'pulsating strains' to describe part of this phenomenon, but it is unclear why his analysis and results are so different from those of Bilby and Kolbuszewski (1977). In neither approach is it a simple matter to compare the finite strain of an initially circular inclusion in simple shear and in pure shear. A comparison between results graphed for simple shear (Bilby and Kolbuszewski, 1977, fig. 6) within one cycle of deformation, and their equation for pure shear, for m values of five and seven, suggests that a significantly *greater* bulk strain is required, to achieve the same amount of distortion of a competent object in simple shear, as in pure shear. This also appears to be the case, when comparing finite element models of elliptical objects in simple shear (M. Casey, pers. comm., 1994) with theoretical values for pure shear. However, according to the analyses of Bilby and Kolbuszewski (1977), the most important differences between object deformations in simple shear and pure shear would be seen for bulk deformations that exceed one cycle of oscillation in simple shear. This would mean comparing deformations with a bulk strain ratio of >100, an excessive strain that is unlikely for pure shear of rocks and may only occur locally in very high strain geological shear zones.

We examine some of these questions further, comparing finite element models of square objects in pure shear and simple shear, where the development of irregular shapes might be expected to be different. In Treagus and Lan (2000), we presented a series of finite element models of square objects in three different orientations (termed 'square', 'rhomb', and 'skew square'), in a matrix undergoing progressive pure shear (Fig. 1), where object and matrix are both Newtonian and have boundary coherence. The objects develop into irregular shapes (Fig. 2), especially the objects 'square' to pure shearing. Objects stiffer than the matrix become barrel-shaped, showing notable concavity of the shortening edges. These are similar to barrel-shaped or 'fish-head' boudins, described by Ramsay (1967, p. 106) and Ghosh (1993, p. 387). In contrast, incompetent objects progressively lose their square outlines, and appear lobate

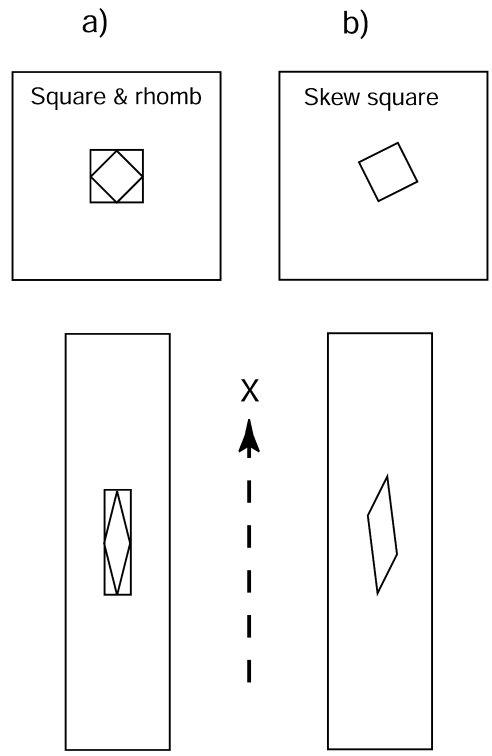

Fig. 1. Design of finite element models of square objects in a matrix, in pure shear, from Treagus and Lan (2000). (a) 'Square' and 'rhomb' models. (b) 'Skew square' model (edges initially inclined at $\tan^{-1}(0.5) = 26.6°$ and $\tan^{-1}(2) = 63.4°$ to pure shear axes (X, Z). The lower figures show the models with passive objects (no viscosity contrast with the matrix) after 50% shortening (X/Z strain ratio of $R = 4$) with the X direction indicated.

and notably rounded. However, square objects diagonal to pure shearing ('rhombs') deform to approximately rhombic shapes, remaining almost straight-sided. The 'skew square model' develops asymmetric shapes between those of 'square' and 'rhomb' models (Fig. 2). These, and many other aspects of shape changes and object deformation, have already been analysed in full in Treagus and Lan (2000).

This paper forms a sequel to Treagus and Lan (2000), and presents comparable finite element models of square objects in a matrix in simple shear. Most of the modelling of object-matrix systems in simple shear has concerned rigid objects of different shapes (Fernandez et al., 1983; Arbaret et al., 2001; Mancktelow et al., 2002; ten Grotenhuis et al., 2002), rather than deformable objects. However, Ghosh and Ramberg (1976, figs. 36–39) provide a few analogue simple shear models of single or grouped deformable square objects with different competence relative to the matrix. Although the viscosity ratios are not quantified (and no incompetent objects are modelled), the ductile competent objects reveal the progressive development of barrelling, similar to those we produced in pure shear numerical models (Fig. 2).

Two questions can be asked of the simple shear models that follow. (1) Do the object shape changes reveal the deformation history and kinematics of the system? If so, these models might be expected to show significant

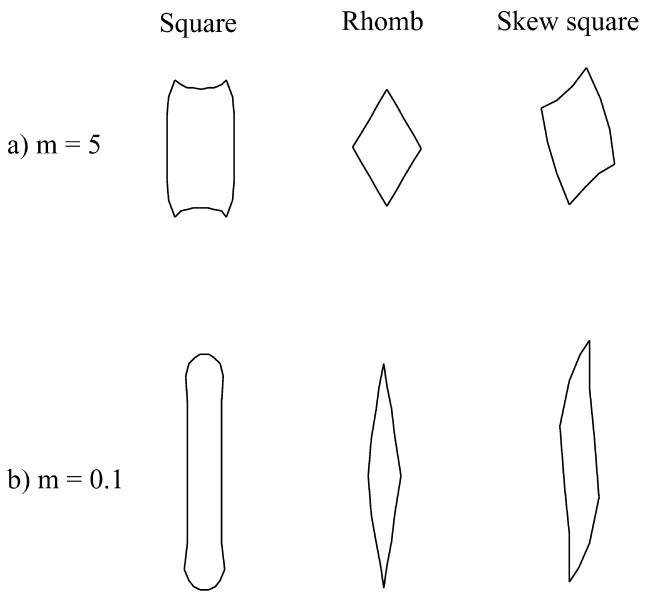

Fig. 2. Selected results of object shape changes (after Treagus and Lan, 2000), for the three types of model shown in Fig. 1. (a) Competent objects, with viscosity ratio of object to matrix of $m = 5$; (b) incompetent objects, with $m = 0.1$.

differences from those in pure shear (cf. Treagus et al., 1996; Treagus and Lan, 2000). (2) Do these simple shear models simulate or mimic any structures that develop in natural shear zones, such as porphyroclast structures commonly used as 'shear criteria' (Simpson and Schmid, 1983; Passchier and Simpson, 1986; Hanmer and Passchier, 1991)?

2. The finite element models

The finite element model we use in this study is a two-dimensional finite element program, developed by Hanson (1990) and modified by Lan and Hudleston (1991), which treats the case of plane, steady-state flow of an ice sheet deforming as an incompressible power-law fluid. A detailed description of the equations and modification of the program can be found in a series of papers (Lan and Hudleston, 1991, 1996, 1997; Hudleston and Lan, 1994).

Hanson (1990) tested the program by comparing the results of finite element simulations with a number of analytical solutions for glaciological problems, achieving good correspondence (to within four digits). However, to have confidence in a complex numerical model, one must verify its performance. The modified program was tested in several ways. This was first done by using it to solve simple problems with known analytical solutions. Good results were obtained (Lan and Hudleston, 1991). Secondly, the numerical results were compared with results of earlier finite element models of structures (folds, faults and mullions) and with theoretical predictions. Again, the correspondence was very good (Lan and Hudleston, 1991). Since then, the program has been used to produce numerous finite element models in the field of structural geology and tectonics, from folding and faulting to objects in a matrix (e.g. Hudleston and Lan, 1993, 1994; Lan and Hudleston, 1996, 1997; Treagus et al., 1996; Treagus and Lan, 2000).

The models in this paper follow almost the same design as the full square model of Treagus and Lan (2000), introduced above (Fig. 1a): but here the deformation is simple shear rather than pure shear (Fig. 3). The same two-dimensional finite element program was used as in the previous studies (Treagus et al., 1996; Treagus and Lan, 2000). In this paper we describe results of comparable modelling in simple shear deformation.

The two-dimensional model (Figs. 3 and 4) comprises a square inclusion (object) enclosed in a surrounding region of matrix, where object and matrix are Newtonian viscous, the object/matrix viscosity ratio is m, and there is perfect coherence at the object-matrix boundary. The design of the model is shown in Fig. 4, and is comparable with the 'square' model of Treagus and Lan (2000, fig. 2a). The whole model is initially 3.4 units square, made up of 449 elements and 444 nodes; the square object is 0.8 units square, comprising 64 small square elements, surrounded by a region of small squares and linking triangular elements that pass into larger squares in the outer region of the matrix. The object occupies 1/18 the model area. The boundary conditions are simple shear, with a fixed base, graduated lateral velocities that maintain $\gamma = 0.025$ per time step, and a constant left-lateral translation of the top (0.085 units per time step). The model thus achieves a bulk simple shear, and retains an overall parallelogram form, as shown in Fig. 3b after 60 time steps ($\gamma = 1.5$). These boundary conditions are equivalent to model 1 of Bons et al. (1997), and comparable with a shear-box experiment. A series of models with different viscosity contrasts were deformed to stages of $\gamma = 0.6$ (24 time increments), $\gamma = 1.15$ (46 increments),

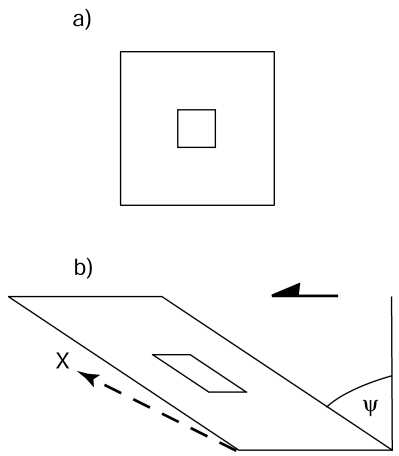

Fig. 3. Design of the finite element simple shear model for a square object in a matrix. (a) Initial model. (b) Model deformed to a shear strain of $\tan\psi = \gamma = 1.5$, which is an X/Z strain ratio of $R_S = 4$. The central square object is passive, with no viscosity contrast with the matrix.

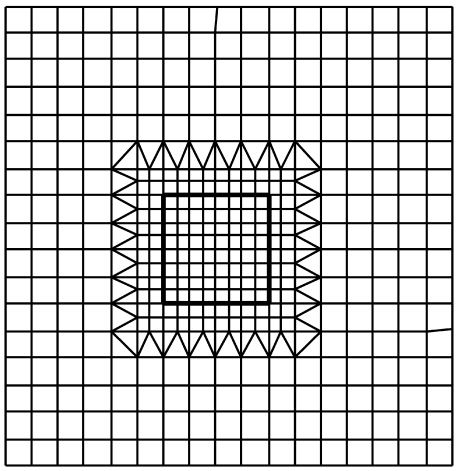

Fig. 4. Initial configuration of elements in the finite element model. The central object with a different viscosity is shown by bold outline.

$\gamma = 1.5$ (60 increments), and $\gamma = 2.7$ (106 increments). Only two models ($m = 5, 0.1$) produced viable solutions for $\gamma = 2.7$. All the models and stages are compiled in Fig. 5.

Regarding the choice of (load) boundary conditions, the velocity boundary condition is used in our model, according to established theory of the finite element method (Zienkiewicz and Taylor, 2000). A great advantage of the velocity boundary is that the model will keep a realistic shape on the loading boundaries, whereas a stress boundary condition would distort the load boundaries to become curved or zigzag. Numerous tests have shown that the stress effect caused by the velocity boundary condition *only* appears in elements along the velocity load boundary; the stress distribution in all other elements away from the boundary is the same as that used by the stress boundary.

The model configuration does not pretend to be simulating a truly isolated inclusion in an infinite matrix, but a square inclusion in a *finite* matrix, to simulate simple shear in rocks containing clasts of a certain spacing. Repetition (tiling) of this model would simulate object-matrix systems with centre spacing ~4-times the object dimension. This size of object, relative to spacing, is considered realistic for rocks containing 'spaced' clasts of various types.

The purpose of these models is to investigate the change in shape of square objects of different viscosity in a matrix, in progressive simple shear; and to compare the results with those described for same-sized models in pure shear (Treagus and Lan, 2000). Importantly, the model for simple shear of $\gamma = 1.5$ achieves an identical bulk strain (X/Z strain ratio of $R_S = 4$) to the pure shear 'skew square' model with $R_S = 4$, introduced earlier (Fig. 1b). This can be confirmed numerically and by comparing the deformed shape of a passive square object, relative to the principal strain directions, seen to be mirrored in Figs. 1b and 3b. We will compare the deformed shapes for models with viscosity contrasts in the next section.

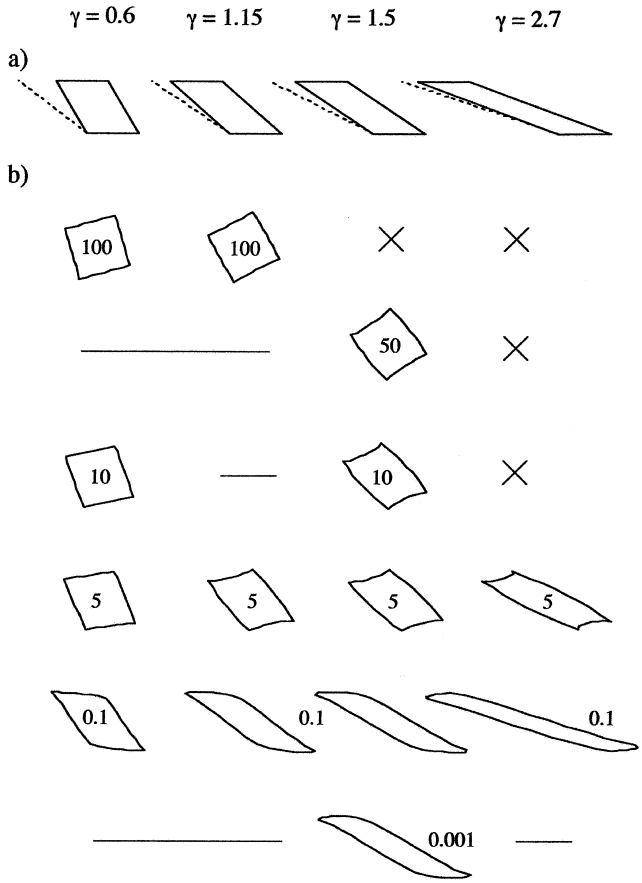

Fig. 5. Shape changes of square objects in a matrix in progressive sinistral simple shear with shear strains of $\gamma = 0.6$, 1.2, 1.5 and 2.7 (columns). (a) Passive objects deform to parallelograms, indicating the bulk simple shear. Dotted lines show orientation of the extension direction (X). (b) Series of models with viscosity contrast (m) labelled. Horizontal lines show γ values not examined; crosses indicate models where viable solutions were not obtained. See text for descriptions of shapes.

3. Analysis of model results

3.1. Object shapes

Fig. 5 reveals the object shape-change from initially square, for all our simple shear models, with different viscosity ratios and different stages of bulk simple shear. The change of shape for a passive square object (no viscosity contrast) is shown progressively in Fig. 5a (cf. Fig. 3b), on which we superimpose the direction of maximum extensional strain (X). This object changes progressively to a parallelogram, in the same manner of the bulk sinistral simple shear. At the highest strain ($\gamma = 2.7$), the original vertical edge is almost parallel to X. Models with different viscosity contrasts (m) are shown in Fig. 5b, in columns of equivalent stages of shear strain (γ).

For the model with $m = 100$, numerical solutions were only found for γ stages up to 1.2. The object records rotation, but no significant distortion. Whether this behaviour is equivalent to the theoretical behaviour of a properly rigid square inclusion will be addressed later. A higher bulk

shear strain ($\gamma = 1.5$) was reached for $m = 50$, and this model shows slight object distortion into a barrel-shape, plus rotation. Heterogeneous strain is more obviously revealed in the $m = 10$ models, producing asymmetric barrel shapes (Fig. 5). The significant effect is progressive concavity of the shortening edge, and convexity of the lengthening edge, as described for pure shear models (Treagus and Lan, 2000). This is even more obvious for the $m = 5$ series, and their progressive shape changes are shown in more detail in Fig. 6. These asymmetric barrel shapes are similar to those of 'skew squares' in pure shear (Fig. 2a). Similar shapes are illustrated by Ghosh and Ramberg (1976) in analogue simple shear models with single or multiple deformable competent objects. In all the numerical models with $m > 1$, the competent objects show a smaller object strain than passive objects, they develop concavity of the shortened edges, and the positions of their original square corners remain obvious.

We use a model series with $m = 0.1$ to illustrate the different effects for incompetent square objects (Fig. 5b), shown in more precise detail in Fig. 7. Now, the object deforms *more* than a passive object, and becomes progressively smoother and curvaceous, due to convexing of the shortening edge. Via an early 'lemon' shape, the original square corners become progressively less clear, until the most deformed objects appear like swimming 'fish' in the direction of simple shear (Fig. 7). Again, the shapes are very similar to those described earlier from pure shear models (Fig. 2b). The previous results for pure shear revealed very similar shapes for incompetent objects in the range of $0.5 > m > 0$. This is confirmed by the simple shear models, and shown by virtually identical object shapes

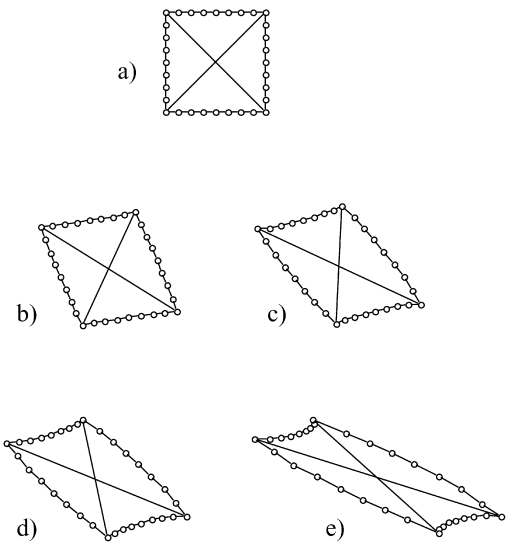

Fig. 6. Detail of the $m = 5$ competent model series. (a) The undeformed square object with the finite element nodes indicated (circles) and two diameters shown. Progressive shape changes are shown for sinistral simple shear with (b) $\gamma = 0.6$, (c) $\gamma = 1.2$, (d) $\gamma = 1.5$ and (e) $\gamma = 2.7$. Note the asymmetric barrel shapes, characterised by two concave shortened edges and two slightly convex lengthened edges.

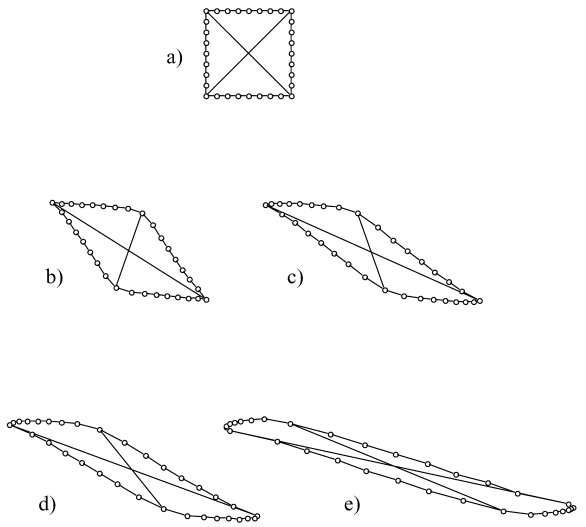

Fig. 7. Detail of the $m = 0.1$ incompetent model series. (a) The undeformed square object with the finite element nodes indicated (circles) and two diameters shown. Progressive shape changes are shown for sinistral simple shear with (b) $\gamma = 0.6$, (c) $\gamma = 1.2$, (d) $\gamma = 1.5$ and (e) $\gamma = 2.7$. Note the progression of asymmetric lemon to fish to ribbon shapes, eventually characterised by two extremely shortened convex leading edges, two almost straight lengthened edges, and blurring of the corners.

arising for $m = 0.1$ and 0.001 at $\gamma = 1.5$ (Fig. 5). Accordingly, we have not illustrated any other incompetent models. What is most distinct about these shapes is the progressive opening out and eventual disappearance of two of the original square corners (Fig. 7).

3.2. Object strain, and comparisons with pure shear models

An important general principle for the simple shear models, is that these material objects occupy progressively different orientations with respect to the non-material bulk principal strain axes, during deformation. The square object modelled has two sides parallel to the direction of simple shear (Fig. 3a), and so the diagonals are initially parallel to the incremental X and Z strain directions. Thus its earliest deformation is comparable with the pure shear 'rhomb' models (Figs. 1 and 2) (Treagus and Lan, 2000). However, the vorticity of the simple shear deformation potentially takes the deforming square into progressively smaller angles to the finite X direction, over time, changing its symmetry with respect to incremental strain.

At $\gamma = 1.5$ ($R_S = 4$), the simple shear model (Fig. 3) has been shown earlier to be 'equivalent' to the deformation of pure shear 'skew square' model with $R_S = 4$, plus rotation (Fig. 2b). This is shown by the shape similarities of the $\gamma = 1.5$ column in Fig. 5, with the pure shear models reproduced in Fig. 8. However, the simple and pure shear models differ slightly in the numbers of nodes that outline their objects (with a greater number of points in the simple shear models producing subtler shape irregularities), and in the object size relative to the whole model (cf. Figs. 1 and 3), with the 'skew square' pure shear model object having

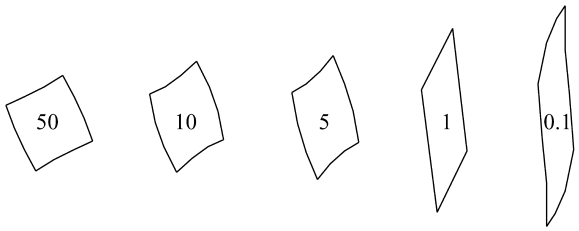

Fig. 8. Object shapes developed in pure shear for the 'skew square' model (Fig. 1b) for viscosity contrasts of 50–0.1 (labelled), and bulk strain of $R_S = 4$, after Treagus and Lan (2000). These can be compared (if mirrored) with models in simple shear at equivalent bulk strain, shown in the $\gamma = 1.5$ column of Fig. 5.

object/model dimension of 1: 4.8, compared with 1:4.25 for these simple shear models. Comparisons of earlier pure shear models with different object sizes has revealed increasing strain in competent objects with decreasing object:model size, and decreasing strain for incompetent objects. However, comparison of the quarter models (dimension ratio 1:6) and full square models (1:4) in Treagus and Lan (2000), for equal bulk strain of $R_S = 4$, shows differences in object strain ratio (R) of only ± 0.1 to 0.2. On this basis, the size-related differences between the pure shear and simple shear models (Figs. 5 and 8) would be expected to be even smaller, probably within ± 0.1 in object R value.

We scaled and enlarged comparable pure shear and simple shear models for precise comparison, and analysed the object shapes using *NIH Image* (the US National Institute of Health Mac-based image analysis software: http://rsb.info.nih.gov/nih-image/). This method determines an object strain for each model, using the analysis function of *NIH Image* to a best-fit ellipse. The results are shown in Fig. 9 as strain ratios and orientations, relative to the bulk

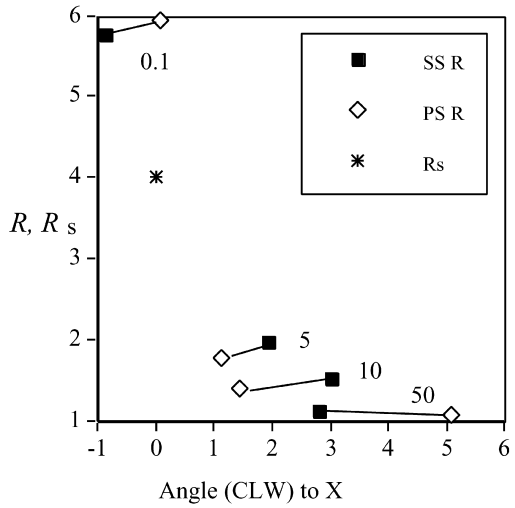

Fig. 9. Comparison of computed object strain for simple shear and pure shear models, using *NIH Image* analysis of best-fit ellipses to the irregular object shapes. R_S is the model (bulk) strain ratio (X/Z), and R the object strain axial ratios, with SS R indicating the simple shear models, and PS R the pure shear models. Angles are measured to bulk X, positive angles measured clockwise. Tie-lines link 'equivalent' simple and pure shear models for the same viscosity contrast (numbered).

strain of $R_S = 4$. As expected from the size differences discussed above, the simple shear models undergo a slightly greater competent object strain for $m = 50$, 10 and 5, by $+0.1$ to 0.2 in R, compared with the pure shear models. Conversely, there is a smaller incompetent object strain (-0.13) for $m = 0.1$. Without further modelling, we cannot be certain of the reason(s) for the differences between these simple shear and pure shear models: whether due to the subtle size and shape differences, or the degree of coaxiality of the deformation, or expected slight differences in *NIH Image* analysis by ellipse approximations of the irregular outlines. However, if the differences are due to the degree of coaxiality of the deformation, this must be a very small effect for this amount of finite deformation.

The orientations of best-fit object ellipse long axes for the simple shear models fall within -1 to 3° clockwise of the bulk stretch, X (Fig. 9). The differences in strain orientation between simple shear and pure shear are small, falling within $\sim 2°$, and are not consistent in sense for the competent set. These also probably reveal differences in *NIH Image* analysis and ellipse fitting of the different irregular object shapes. In conclusion, therefore, we do not find significant differences between the object shapes and strains in simple shear and pure shear, sufficient to indicate the type of bulk deformation.

A more detailed analysis of object strain is given in Fig. 10, for the progressive simple shear models shown in detail in Figs. 6 and 7 ($m = 5$ and 0.1, respectively). The strain analysis is made using *NIH Image*, as described above, to determine an R_S value for the best-fit strain ellipse for each object, with θ denoting the orientation of ellipse long axes to the shear direction. As expected, a generally greater strain is revealed for the incompetent objects, compared with the bulk strain, for each model stage. Conversely, there is a smaller strain for the competent objects. The positions of the curves, relative to the asterisks that show the bulk simple shear, reveal that the incompetent strain cannot be considered simply as a greater amount of simple shear, nor the competent strain a weaker simple shear. The differences in R values for the different viscosity contrasts are much more significant than the differences in the principal axial axial orientation, θ.

3.3. Object rotations

For the objects in simple shear, examined in the preceding section, it is not a trivial matter to separate rotations related to object strain from 'rigid' rotation. If the stiff square inclusions had behaved as truly rigid objects, and rotated in two dimensions in the manner of circular objects in an infinite matrix in simple shear (Jeffery, 1922; Ghosh and Ramberg, 1976), their incremental rotation would be constant, and the finite angle of rotations (ω) would be given by:

$$\omega = \gamma/2 \text{ (in radians)} \quad (1)$$

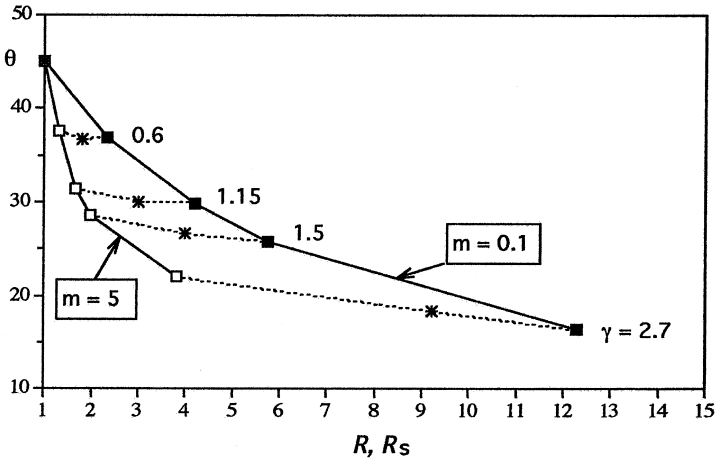

Fig. 10. Strain analysis of the models shown in Fig. 6 ($m = 5$) and Fig. 7 ($m = 0.1$), using *NIH Image* analysis of best-fit ellipses to the irregular object shapes. R indicates object strain ellipse axial ratios, and θ the orientation of ellipse long axis to the shear direction. Asterisks indicate the model (bulk) strain ratio (R_S), and dotted tie-lines join values for successive amounts of bulk simple shear (γ values numbered).

(Ghosh, 1993, p. 211). Fig. 11 shows the theoretical rotation of rigid square objects according to Eq. (1), using a diagonal as a marker. Eq. (1) is also shown as the linear relationship of ω to γ in Fig. 12.

We are unaware of any theoretical proof that square objects follow the same rotations as circles, but several analogue studies have used square, rectangular or elongate monoclinic (rhomboid) rigid objects to test the analytical expressions for the rotation of rigid elliptical objects in simple shear (Fernandez et al., 1983; Arbaret et al., 2001; Mancktelow et al., 2002; ten Grotenhuis et al., 2002), and have found good data fits to ellipses.

Returning to the comparisons between models of simple and pure shear discussed earlier, we find in Eq. (1) that for a simple shear of $\gamma = 1.5$, $\omega = 43°$, and so the square diagonal (Fig. 11) is 2° clockwise of the shear direction, 24.6° counterclockwise of the X direction. In pure shear, the equivalent 'skew square' model does not rotate, and (when mirrored, for comparison) its diagonal is 18.4° counter-clockwise of X. Thus, according to theory for isolated objects, there would be about 6° more rotation for rigid circles and squares (in an infinite matrix), in simple shear than in pure shear with equivalent bulk strain ($R_S = 4$).

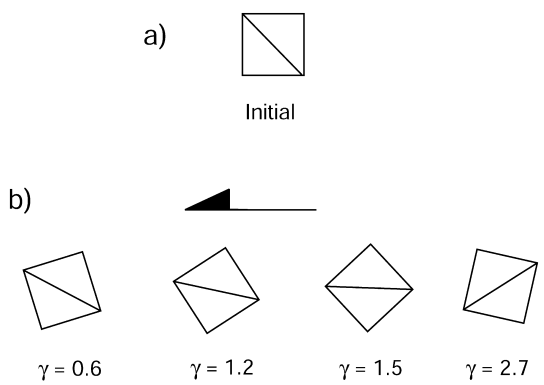

Fig. 11. Theoretical rotation of a rigid square object (a), in sinistral simple shear with increasing γ (b), according to Eq. (1) and γ values shown.

The same object diagonal (cf. Fig. 11) can now be used to measure rotations in the simple shear models (Figs. 4–6), to compare these results with rigid objects and with a passive diagonal marker. Results for different m values (Fig. 12) reveal positions progressively closer to the passive marker, with reducing viscosity contrast. The stiffest modelled objects ($m = 100$) do not rotate as much as ideal theoretical rigid objects, despite showing negligible strain. This is probably a result of the finite size of the model compared with infinite matrix theory. We have not varied the object size relative to matrix in the finite element simple shear models, to examine the size effect on 'rigid' rotation. However, Marques and Coelho (2001) examined the rotational behaviour of rigid elliptical objects, in shear zones of varying widths relative to the object size. For a shear zone whose width relative to object short axis (termed S) is given by $S = 3.5$, an object with axial ratio of 1.5 rotates consistently less than the theoretical angle of Ghosh and Ramberg (1976) (see Marques and Coelho, 2001, fig. 4). The analogue experiments used by Ghosh and Ramberg (1976, fig. 5) to confirm their theoretical rotations had S values of about six, so this value might be taken to approximate an isolated object in a semi-infinite matrix. Marques and Coelho do not have experimental results for $S > 3.5$ with circular objects, so there are no direct analogies with our numerical models (equivalent $S = 4.25$), but their trends would suggest a rigid rotation for our stiffest squares ($m = 100$) that is less than the theoretical angles for rigid circular objects (Eq. (1)), as is found in Fig. 12a.

At $\gamma = 1.5$, our $m = 50$ object rotates 30°, compared with 43° rotation for a theoretical rigid object (Fig. 12a). Some of this under-rotation may relate to object:model size, as for $m = 100$. However, some under-rotation is probably due to the slight object deformation in this model (Fig. 5), which prevents it from behaving as effectively rigid. In the range from $m = 10$ to 0.1, the differences in ω are only a few degrees (Fig. 12), and may partly reflect $\pm 1°$ accuracy of

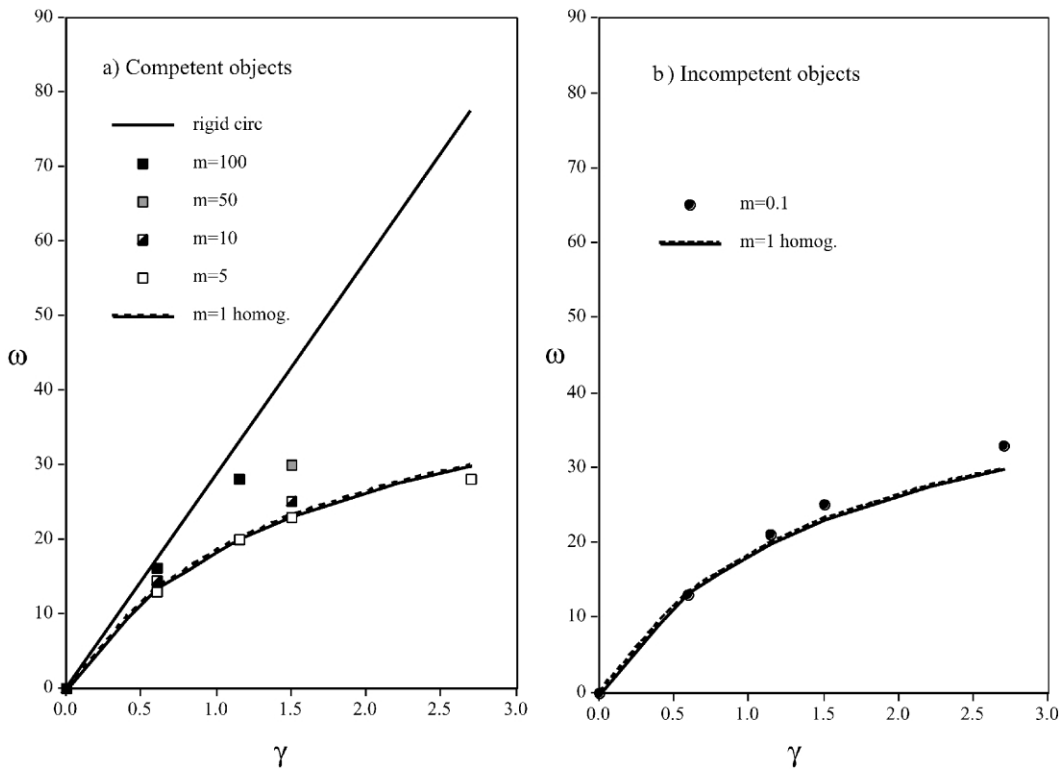

Fig. 12. Angular rotation, ω, for the leading diagonal of a square object (see Fig. 11a) in progressive simple shear of $\gamma = 1$ to 2.7. The broken line shows the rotation of a passive 45° marker, for reference. (a) Competent objects: solid line is the theoretical relationship for rigid equant objects (Eq. (1)); symbols indicate finite element models from Fig. 5, with viscosity ratios (m) as shown. (b) Incompetent $m = 0.1$ objects.

model measurements. Nevertheless, the difference between the $m = 5$ and 0.1 models at $\gamma = 2.7$ are significant, and not what might be expected. Here, the stiffer object diagonal has rotated *less* than the equivalent passive marker, and the incompetent object rotated more. This feature appears to relate to differences in object strain shown in Fig. 10, rather than reflecting the vorticity of the deformation, and is also indicated by the larger angle of best-fit ellipse long axes to the shear zone for the $m = 5$ object, and smaller angle for the $m = 0.1$ (incompetent) object.

Up to moderate shear strain ($\gamma = 1.5$), and within one order of magnitude of viscosity contrast with the matrix ($m = 10$ to 0.1), the average behaviour of the objects is a rotation of the lengthening diagonal that is very close to passive behaviour, *even when* the strain is markedly different. As noted earlier, these deformable objects also appear to take up orientations with respect to the principal strain axes that are almost indistinguishable from pure shear models, and so do not provide obvious clues to the vorticity of the simple shear deformation.

4. Discussion and geological implications

The simple shear models presented in this paper only reveal the behaviour of one orientation of a square object with varying viscosity contrast to the matrix. All the objects were initially aligned with the shear direction. Squares oriented with their sides at other angles will deform into different shapes from those shown in Figs. 5–7, occupying a full range from barrel shapes to rhomboids (competent) or bone shapes to rhomboid (incompetent), as shown in detail for pure shear (Treagus and Lan, 2000) (e.g. Fig. 2). This previous work, and the comparison we have made between pure shear and simple shear models, now allow us to make some extrapolations to square objects with other orientations to the shear direction, such as diagonal squares.

A comparison of the deformation of squares and diagonal squares in simple shear is shown schematically in Fig. 13. We choose a shear strain of $\gamma = 1.5$ for illustration, and choose $m = 5$ for competent and $m = 0.1$ for incompetent objects. The behaviour of *passive objects* is shown in Fig. 13b; as deformation is, by definition, homogeneous, the strain trajectories (X; dashed lines) are straight. The *competent objects* (Fig. 13c) are both asymmetric barrels. The left 'square' is after Fig. 6d; the right 'diagonal square' uses the coordinates of side midpoints from Fig. 6d to define the object corners, and the shapes are extrapolated from other models, following principles of *concaving* of shortened edges and *convexing* of elongating edges described earlier. A similar shape is produced by Ghosh and Ramberg (1976, fig. 38) in analogue models of deformable square objects diagonal to shearing. The bulk X direction is indicated, away from the objects, but the strain trajectories would be expected to wrap around the objects, reflecting the

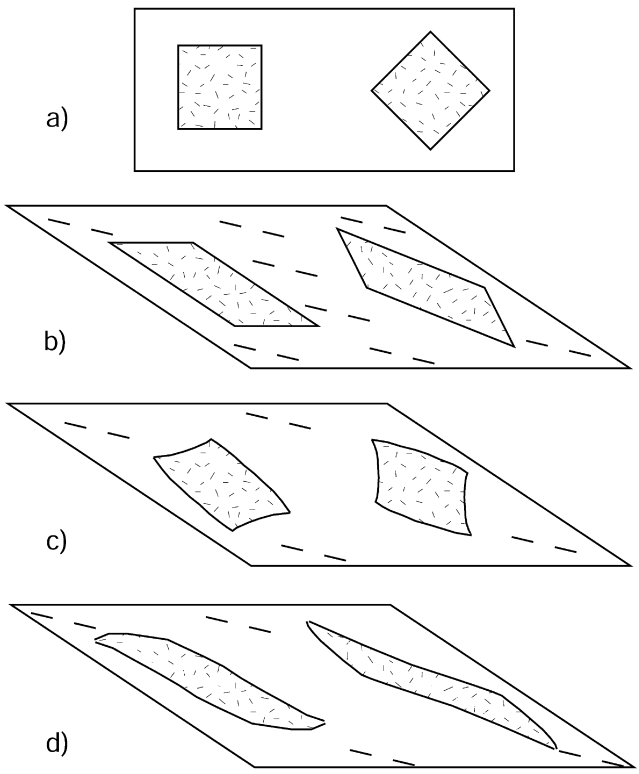

Fig. 13. Modelled and extrapolated shapes of square and diagonal-square objects (a) in a sinistral shear zone with $\gamma = 1.5$. (b) Passive objects deform homogeneously into parallelograms, and a fabric related to the *X* direction of finite strain (dashed lines) would be uniform. (c) Competent objects (viscosity ratio of 5) both develop skew barrel shapes and concave ends. In detail, the fabric in the matrix would be deflected around the objects. (d) Incompetent objects (viscosity ratio of 0.1) develop fish shapes with different asymmetry, but only a small difference in long-axis orientation, acute to the shear direction and at a small angle to the bulk *X* direction.

heterogeneous strain in matrix surrounding competent objects (Ghosh and Sengupta, 1973).

Object shapes of the kind shown in Fig. 13c are commonly associated with the process of boudinage (Ramberg, 1955), particularly where the boudin is ductile and undergoes deformation after fracture separation (Ramsay, 1967, p. 106; Ghosh, 1993, p. 387). However, we show here and elsewhere (Treagus et al., 1996; Treagus and Lan, 2000) that a series or train of angular objects is not required, to reveal these barrel to fish-mouth shapes. The shape features arise in *single* competent objects, as also demonstrated in finite element models of rectangular objects with elastic-plastic rheology by Lloyd and Ferguson (1981), and with viscous rheology by Ramsay and Lisle (2000, fig. 39.19). These authors make direct comparisons with geological boudins.

Barrel or fish-mouth shaped geological clasts with concave shortened edges appear to be rather rare in deformed conglomerates and breccias. During work in progress (with J.E. Treagus), these shapes have been found in occasional clasts in the Brioverian Cesson Conglomerate in Brittany (Treagus and Treagus, 2002), in the Ordovician Letterbrock Conglomerate in Co. Clare, Ireland, and in the Ordovician Porth Wen Conglomerate of N. Anglesey, Wales. However, caution is needed before irregular clasts of this kind can be used as natural illustrations of the barrel shapes modelled in this paper, since it cannot be assumed that the clasts were originally perfectly square, nor that the deformation was simple shear. Several clasts with consistent geometry of concaving and convexing of shortened and lengthened edges, respectively, are needed, before the objects could be reliably used to provide information on the viscosity contrast of the rock, for example according to the concavity factor quantified in Treagus and Lan (2000).

Intriguing examples of barrel-shaped geological objects can be seen in feldspar porphyroblasts in a schist described by Johnson and Williams (1998, fig. 3). Their emphasis was in the phenomenon of 'oppositely concave microfolds', seen when tracing an early schistosity from the schist matrix into inclusion trails near the short edges of feldspar porphyroblasts, and a product of the competence contrast. However, in detail, the porphyroblast outlines reveal barrel shapes and concave shortened edges characteristic of objects 5 or 10 times more viscous than the matrix.

There is a temptation to draw analogies between the asymmetric shapes shown in Fig. 13, and shear criteria (Simpson and Schmid, 1983; Passchier and Simpson, 1986; Hanmer and Passchier, 1991), but we cannot claim that the *shapes* of competent objects, alone, provide evidence of regional shearing. The characteristic features of porphyroclasts that these authors describe (e.g. δ or σ types), are not necessarily associated with objects assumed to be initially square, as in our models; nor can it be assumed that these clasts have a sharp viscosity contrast with the surrounding matrix, as in our models. Instead, porphyroclasts of these types, even if originally rectilinear in shape, may be associated with changes in rheology mantling the clasts, as simulated in analogue models by Passchier and Sokoutis (1993). If the competent objects shown in Fig. 13c involved strain or strain-rate softening in the corner regions of greatest deformation, their shapes over a sustained simple shear would become more exaggerated, more similar to the elastic-plastic models of Lloyd and Ferguson (1981), and might then resemble δ or σ clasts that have been used as shear criteria in natural shear zones. The limit in the amount of shear strain that could be attained in our finite element models also restricts the analogies with natural shear zones that may have undergone very large γ.

In Fig. 13d, similar principles are used to construct the shapes of deformed *incompetent objects* as 'squares' and 'diagonal squares'. Both orientations produce shapes that might be called *fish*: the final alignment of the two orientations is not very different, with the long axis at an acute angle to *X*, but the geometry is reversed. Ghosh and Ramberg (1976) did not model incompetent objects of this kind, and we are unaware of any other models that have produced these shapes in incompetent objects in simple shear. Qualitatively, these fish shapes are remarkably similar to some of the varieties of mineral fish (usually

mica) described in mylonites (e.g. Lister and Snoke, 1984, figs 3–7; Passchier and Trouw, 1996, fig. 5.27; ten Grotenhuis, 2000). These authors illustrate mica fish with geometry of both types shown in Fig. 13d (also Fig. 7), oriented at acute angles to the shear direction. Whether it might be argued that mica fish develop their characteristic shapes when behaving as initially incompetent objects in shear zones, and after a certain stage behave as quasi-rigid objects, and what this might signify for the rheology of shear zones over time, is left open to further investigation.

The modelling and geological discussion above concern objects that are in perfect continuity and coherence with their matrix. Several recent studies have compared the effects of a slipping with a non-slipping interface on the rotation of rigid objects in simple shear (e.g. Ildefonse and Mancktelow, 1993; Marques and Coelho, 2001; Mancktelow et al., 2002), and conclude that the stable orientations of porphyroclasts in shear zones are suggestive of a slipping interface. It is not possible to speculate what the effects and geological implications would be, if the simple shear models in this paper had assumed perfect interfacial slip rather than coherence. However, we consider a coherent object-matrix boundary to be an appropriate model for deformation of many types of rocks, and it still remains for further work to prove when and whether there is uncoupling and interfacial slip around clasts in geological shear zones.

5. Conclusions

Finite element models show that square objects with a viscosity contrast to their matrix deform into a variety of shapes, regardless of whether the deformation is by pure shear or simple shear. Square or more generally angular geological objects (e.g. clasts, porphyroblasts, boudins) might likewise be expected to deform to shapes that are indicative of the viscosity contrast.

We asked two specific question about the simple shear models, at the beginning of this paper. (1) Do the object shape changes reveal the deformation history and kinematics of the system? (2) Do these simple shear models simulate any structures that develop in natural shear zones, such as porphyroclast structures commonly used as 'shear criteria'?

Our answer to the first is that we did not find any characteristic geometries in simple shear that did not also arise for pure shear of square objects in a matrix. However, our direct comparisons between pure and simple shear have been restricted to $\gamma = 1.5$. The special characteristics of simple shear in terms of cycles of oscillating strain and rotation, given by the theory of Bilby and Kolbuszewski (1977), require significantly greater shear strains; for example, one cycle of 'bounded deformation' for $m = 7$ requires $\gamma \cong 10$. We therefore conclude that the structural and mechanical differences between simple shear and pure shear will only be properly revealed at high finite strain ($R_S \gg 4$). Other structural associations, such as strain heterogeneity and localised high-strain shear zones, will provide better clues to simple shear than will strained objects alone.

In answer to the second question, and following on from arguments above, we consider that the geometry of deformed square objects alone will not be sufficient to deduce a shear zone and sense of shear. However, in an identified shear zone that possesses a consistent asymmetry of porphyroclasts of various kinds, shapes such as those shown in Fig. 13 would be a good indicator of sinistral shear. Potentially the most interesting outcome of the modelling in this paper is the development of shapes in incompetent objects that are similar to mica fish described in mylonite zones. Whether this is accidental or significant of their mechanism will be pursued in other work.

We conclude that there may be non-uniqueness to many features of natural deformation arising from pure shear and simple shear, up to moderate strain. For square objects in a matrix, the object shape change principally depends on its rheological contrast with the matrix. Properties such as non-Newtonian flow laws, material anisotropy and a slipping object-matrix boundary, will also influence the deformation of objects in a matrix, and are topics for further work.

Acknowledgements

This paper was written while S.H.T. was in receipt of a NERC Senior Research Fellowship, which is gratefully acknowledged. We would like to thank Jack Treagus for his support and comments, and John Dewey for encouraging our work on the Letterbrock Conglomerate. Thanks are due to Paul Bons and Fernando Marques for their thorough reviews, which have led to significant changes to the manuscript.

References

Arbaret, L., Mancktelow, N.S., Burg, J.-P., 2001. Effect of shape and orientation on rigid particle rotation and matrix deformation in simple shear flow. Journal of Structural Geology 23, 113–125.

Bilby, B.A., Eshelby, J.D., Kundu, A.K., 1975. The change of shape of a viscous ellipsoidal region embedded in a slowly deforming matrix having a different viscosity. Tectonophysics 28, 265–274.

Bilby, B.A., Kolbuszewski, M.L., 1977. The finite deformation of an inhomogeneity in two-dimensional slow viscous incompressible flow. Proceedings of the Royal Society A 355, 335–353.

Bons, P.D., Barr, T.D., ten Brink, C.E., 1997. The development of δ-clasts in non-linear viscous materials: a numerical approach. Tectonophysics 270, 29–41.

Eshelby, J.D., 1957. The determination of the elastic field of an ellipsoidal inclusion, and related problems. Proceedings of the Royal Society A 241, 376–396.

Fernandez, A., Feybesse, J.-L., Mezure, J.-F., 1983. Theoretical and experimental study of fabrics developed by different shaped markers in two-dimensional simple shear. Bull. Soc. Géol. France 25, 319–326.

Freeman, B., 1987. The behaviour of deformable ellipsoidal particles in

three-dimensional slow flows: implications for geological strain analysis. Tectonophysics 132, 297–309.
Gay, N.C., 1968a. Pure shear and simple shear deformation of inhomogeneous viscous fluids. 1. Theory. Tectonophysics 5, 211–234.
Gay, N.C., 1968b. Pure shear and simple shear deformation of inhomogeneous viscous fluids. 2. The determination of the total finite strain in a rock from objects such as deformed pebbles. Tectonophysics 5, 295–302.
Ghosh, S.K., 1993. Structural Geology. Fundamentals and Modern Developments, Pergamon Press, Oxford.
Ghosh, S.K., Ramberg, H., 1976. Reorientation of inclusions by combination of pure and simple shear. Tectonophysics 34, 1–70.
Ghosh, S.K., Sengupta, S., 1973. Compression and simple shear of test models with rigid and deformable inclusions. Tectonophysics 17, 133–175.
Hanmer, S., Passchier, C.W., 1991. Shear sense indicators: a review. Geological Survey of Canada Paper 90-17.
Hanson, B.H., 1990. Thermal response of a small ice cap to climatic forcing. Journal of Glaciology 36, 49–56.
Hobbs, B.E., Means, W.D., Williams, P.F., 1976. An Outline of Structural Geology, John Wiley & Sons, New York.
Hudleston, P.J., Lan, L., 1993. Information from fold shapes. Journal of Structural Geology 15, 253–264.
Hudleston, P.J., Lan, L., 1994. Rheological controls on the shapes of single-layer folds. Journal of Structural Geology 16, 1007–1021.
Ildefonse, B., Mancktelow, N.S., 1993. Deformation around rigid particles: the influence of slip at the particle/matrix interface. Tectonophysics 221, 345–359.
Jeffery, G.B., 1922. The motion of ellipsoidal particles immersed in a viscous fluid. Proceedings of the Royal Society Series A 102, 161–179.
Johnson, S.E., Williams, M.L., 1998. Determining finite longitudinal strains from oppositely-concave microfolds in and around porphyroblasts: a new quantitative method. Journal of Structural Geology 20, 1521–1530.
Lan, L., Hudleston, P.J., 1991. Numerical models of buckle folds in non-linear materials. Tectonophysics 199, 1–12.
Lan, L., Hudleston, P.J., 1996. Rock rheology and angular folds in single-layers. Journal of Structural Geology 18, 925–931.
Lan, L., Hudleston, P.J., 1997. Numerical simulation of fault-bend folds in fold-and-thrust belts. Proceedings of the 30th International Geological Congress V4, 106–118.
Lisle, R.J., Rondeel, H.E., Doorn, D., Brugge, J., van de Gaag, P., 1983. Estimation of viscosity contrast and finite strain from deformed elliptical inclusions. Journal of Structural Geology 5, 603–609.
Lister, G.S., Snoke, A.W., 1984. S–C mylonites. Journal of Structural Geology 6, 617–638.
Lloyd, G.E., Ferguson, C.C., 1981. Boudinage structure: some new interpretations based on elastic-plastic finite element simulations. Journal of Structural Geology 3, 117–128.
Mancktelow, N.S., Arbaret, L., Pennacchioni, G., 2002. Experimental observations on the effect of interface slip on rotation and stabilisation of rigid particles in simple shear and a comparison with natural mylonites. Journal of Structural Geology 24, 567–585.
Marques, F.O., Coelho, S., 2001. Rotation of rigid elliptical cylinders in viscous simple shear flow: analogue experiments. Journal of Structural Geology 23, 609–617.
Marques, F.O., Coelho, S., 2003. 2-D shape preferred orientations of rigid particles in transtensional viscous flow. Journal of Structural Geology 25 in press.
Passchier, C.W., Simpson, C., 1986. Porphyroclast systems as kinematic indicators. Journal of Structural Geology 8, 831–843.
Passchier, C.W., Sokoutis, D., 1993. Experimental modelling of mantled porphyroclasts. Journal of Structural Geology 15, 895–909.
Passchier, C.W., Trouw, R.A.J., 1996. Microtectonics, Springer, Berlin.
Ramberg, H., 1955. Natural and experimental boudinage and pinch-and-swell structures. Journal of Geology 63, 512–526.
Ramsay, J.G., 1967. Folding and Fracturing of Rocks, McGraw Hill, New York.
Ramsay, J.G., Lisle, R.J., 2000. The Techniques of Modern Structural Geology. Volume III. Applications of Continuum Mechanics in Structural Geology, Academic Press, London.
Shimamoto, T., 1975. The finite element analysis of the deformation of a viscous spherical body embedded in a viscous medium. Journal of the Geological Society of Japan 81, 255–267.
Simpson, C., Schmid, S.M., 1983. Evaluation of criteria to deduce the sense of movement in sheared rocks. Geological Society of America Bulletin 94, 1281–1288.
ten Grotenhuis, S.M., 2000. Mica fish in mylonites. Ph.D. thesis (unpublished), Johannes Gutenberg Universität Mainz, Germany.
ten Grotenhuis, S.M., Passchier, C.W., Bons, P.D., 2002. The influence of strain localisation on the rotation behaviour of rigid objects in experimental shear zones. Journal of Structural Geology 24, 485–499.
Treagus, S.H., Lan, L., 2000. Pure shear deformation of square objects, and applications to geological strain analysis. Journal of Structural Geology 22, 105–122.
Treagus, S.H., Treagus, J.E., 2002. Studies of strain and rheology of conglomerates. Journal of Structural Geology 24, 1541–1567.
Treagus, S.H., Hudleston, P.J., Lan, L., 1996. Non-ellipsoidal inclusions as geological strain markers and competence indicators. Journal of Structural Geology 18, 1167–1172.
Weijermars, R., 1993. Pulsating strains. Tectonophysics 220, 51–67.
Zienkiewicz, O.C., Taylor, R.L., 2000. The Finite Element Method: Volume 1. The Basis, Butterworth-Heinemann, Oxford.